Pyrolysis Kinetics of *Spirulina platensis* and Non-condensable Gas Product Distribution in a Fixed-Bed Reactor

Ahmad Yusril Aminullah[1], Sukarni Sukarni[1,2,*], Retno Wulandari[1], Muhammad Shahbaz[3,4]

[1]*Center for Renewable Fuels Research (CRFR), Department of Mechanical and Industrial Engineering, Universitas Negeri Malang, Indonesia*
[2]*Center for Advanced Material for Renewable Energy (CAMRY), Universitas Negeri Malang, Indonesia.*
[3]*Net Zero Industry Innovation Centre, School of Computing, Engineering and Digital Technologies, Teesside University, Middlesbrough, United Kingdom.*
[4]*College of Science and Engineering, Hamad Bin Khalifa University, Education City, Doha, Qatar.*
**Corresponding author: sukarni.ft@um.ac.id*

Article history:
Received: 1 June 2024 / Received in revised form: 12 July 2024 / Accepted: 16 July 2024
Available online 20 July 2024

ABSTRACT

Energy is a fundamental factor for civilization development and sustainability. However, energy sources are dominated by non-renewable fractions, such as fossil fuels. Renewable biomass is projected to be a future fuel source. *Spirulina platensis* (SP) has numerous advantages compared to other biomass, and it is considered 3rd generation biomass that does not interfere with food and land usage and has a relatively low main decomposition temperature at 325.7℃. Thermogravimetric analysis (TGA) was conducted to observe SP kinetics parameters, especially activation energy. Kissinger-Akahira-Sunose (KAS), Ozawa-Flynn-Wall (OFW), and Starink iso-conversional methods reveal that SP has an activation energy of 152.33, 154.56, and 152.78 kJ/mol, respectively. The coefficient correlation (R^2) of OFW is the highest compared to its counterpart at 0.9918. Non-condensable gas (H_2, CH_4, and CO_2) product distribution is characterized using a fixed-bed pyrolysis reactor. The average concentrations of H_2, CH_4, and CO_2 are 3775.2, 83792.19, and 23592.58 ppm, in that order. H_2 production is linked with carbohydrates and protein decomposition. CH_4 yield heavily depends on protein degradation, followed by carbohydrates and lipids. CO_2 yield mainly originated from carbohydrate cracking. The optimum SP pyrolysis temperature is 310—370℃ based on its non-condensable gas yield, TGA result, OFW kinetics method, and thermodynamics parameter, where it has relatively low activation energy (139.29 kJ/mol) accompanied by a significant increase of non-condensable-gas-production.

Keywords: *Iso-conversional, kinetics, non-condensable gas, pyrolysis, Spirulina platensis*

I. Introduction

Energy is a basic driver of human civilization and technological progress. The growing global population and modern lifestyle have increased energy demand, which is still going on [1]. However, fossil fuel reserves, being finite and major contributors to environmental damages resulting in climate change, are unable to meet these escalating demands in a sustainable manner [2]. Efforts are ongoing to restrict the rise of global temperature to below 2°C, such as the Doha Protocol and COP26, where most countries agreed to achieve this target [3]. This effort is directly associated with decreasing reliance on fossil fuels by incorporating more sustainable and low-carbon footprint energy sources. To support this goal, the United Nations has established 17 Sustainable Development Goals (SDGs), providing a comprehensive framework to address global temperature rise and restore

DOI: 10.17977/um016v8i12024p151

conditions to pre-industrial levels [4]. In this scenario, scientists, policymakers, and energy-producing and providing enterprises are exploring various energy production options such as solar, geothermal, wind, and biomass-based energy [5].

Among all sustainable energy avenues, biomass stands out as one of the most important due to its renewability, carbon neutrality, ability to produce multiple energy products (such as hydrogen, diesel, and biogas), and many value-added products. This provides a comprehensive biorefinery concept, offering an alternative to products traditionally obtained from fossil fuel-based refineries [6]. Biomass is a non-fossilized source known as renewable biomass resources, including forest residue, non-edible seeds, agricultural residue, and advanced biomass such as microalgae, which are acknowledged for their sustainability and carbon neutrality [1]. There are two main ways to extract energy from biomass: biological and thermochemical conversion processes. Biomass is the only source capable of producing liquid, solid, and gaseous fuels [7]. Thermochemical processes are the most efficient means of converting biomass into renewable fuels [2]. These processes, including combustion, gasification, hydrothermal liquefaction, and pyrolysis, are the major thermochemical techniques aiming to degrade higher molecular weight compounds into lower molecular weight ones under the influence of heat [8]. Consequently, volatile products are released, generating various gases such as hydrogen, methane, carbon dioxide, and trace amounts of other hydrocarbon gases.

The cyanobacterium *Spirulina platensis* (SP) is a species of blue-green algae that grows in freshwater or brackish habitats. It can also be found in marine regions in the equatorial and tropical zones [9], [10]. Algae cultivation can also be done on non-arable soils, in contrast to typical crops, which require arable land. Furthermore, microalgae may be grown in wastewater with far less water than terrestrial plants, easing freshwater scarcity [11]. Algae are photoautotrophs that require sunlight, CO_2, and water and contain small amounts of mineral salts. Microalgae could be characterized by high-efficiency photosynthesis; theoretically, microalgae may be more efficient than terrestrial plants due to their relatively simple structure and immersion in the nutrient solution [12]. These microalgae are relatively large in size, which makes it easier and economical to harvest them by filtering the medium [13]. Algal technologies provide options for long-term CO_2 capture and sequestration. These include burying carbon-rich fractions derived from biomass, leading to CO_2 neutrality along with lower emission of other pollutants into the environment [11].

SP is common and prolific in Indonesia because of its vast oceanic area. It could be a very good source for producing bioenergy and value-added products through both biological and thermal conversion processes. This is due to its numerous benefits, such as abundant availability, carbon neutrality, year-round availability, and good calorific values. At the same time, a number of studies have examined the thermal properties of SP for pyrolysis-based feedstock and its promising gas product yield [9], [11], [14]–[16]. Pyrolysis is an important process for producing liquid and gaseous products. To utilize SP in a tailored pyrolysis reactor process, it is very beneficial to determine the thermal properties and thermal kinetics using a thermogravimetric analyzer, which also provides the pyrolysis environment and conditions [17]. However, pyrolysis temperature plays a vital role in energy usage, economics, and desired product yield efficiency.

Thermal decomposition and reaction kinetics of biomass are often studied utilizing thermogravimetric analysis (TGA) to obtain optimum pyrolysis temperature [18]. Kinetics parameters and pyrolysis mechanisms are determined using TGA data through various mathematical approaches [19]. Biomass thermal degradation follows both the single-step

global model and the Arrhenius equation, later differentiated into iso-conversional methods such as Kissinger-Akahira-Sunose (KAS), Ozawa-Flynn-Wall (OFW) and Starink representing kinetics parameters during the reaction. Soen et al. [20] found that model-free iso-conversional methods had a better approach than model-based methods and required less mathematical proficiency compared to distributed activation methods. TGA also provides an estimated production of gaseous products at a specific temperature through its derivative graph [21]. Nevertheless, TGA alone cannot determine non-condensable gas distribution. Suprianto et al. [22] employ an MQ-series sensor to detect sawdust pyrolysis gas product species. Pyrolysis temperature dictates the occurrence of reactions that affect product yield and gas composition [23]. Combining TGA with non-condensable gas composition analysis provides an overview of the pyrolysis potential to produce H_2-rich non-condensable gas along with other products. Non-condensable gas production is directly correlated with kinetics parameters. Yacob et al. [24] reveal that gas products from human feces pyrolysis consisting of H_2, CH_4, CO_2, CO, and C_2H_6 are linked with kinetics parameters, especially activation energy, where kinetics modeling is required to optimize the biomass pyrolysis process. Another study done by Qin et al. [25] also found that gaseous products of medical waste pyrolysis consisting of H_2, CH_4, C_2H_2, C_2H_4, and C_2H_6 are formed with the activation energy of 65.1, 39.98, 35.17, 38.71, and 40.75 kJ/mol. However, kinetic parameter and gas product distribution correlation still lack literature, and studies about SP kinetics and non-condensable gas yield correlation has not been deducted, where it can be useful to determine optimum SP pyrolysis temperature.

From the above discussion, it can be concluded that thermal degradation studies are very important for understanding reaction kinetics and the composition of pyrolysis products, such as gaseous outputs. The novelty of this study lies in its clear definition of the correlation between activation energy, thermodynamics parameters, and the pyrolysis process for gas production, a relationship that has not been reported previously. The thermal degradation of SP has been minimally investigated, especially concerning its gas composition through the pyrolysis process. The aim of this investigation is to study the thermal degradation of SP at heating rates of 10, 20, 30, and 40 °C/min and to perform the model-free iso-conversional of KAS, OFW, and Starink. The most suitable model-free method based on its coefficient correlation (R^2) is employed to calculate thermodynamic parameters. The second and most important objective is to perform the pyrolysis of SP in a tailored fixed-bed reactor to determine the non-condensable gas composition and evaluate its production.

This study will provide valuable information on the basic kinetic and thermal properties as well as the non-condensable gas potential from the pyrolysis process, which will be helpful for further designing efficient pyrolysis reactor parameters based on SP optimum degradation temperature and support efforts towards carbon-neutral approaches.

II. Material and Methods

1. Biomass Feedstock

Commercially available Spirulina microalgae were used as pyrolysis feedstock. Spiruganik+^{TM} spirulina (SP) was purchased from Tangerang, West Java, Indonesia. SP powder was then filtered using a mesh size of 60 and kept in a desiccator. It was stored in an airtight jar.

2. Experimental Setup and Procedure

The system has been used for the conversion of SP into non-condensable gas via the pyrolysis process is presented in Figure 1. The system consists of a fixed-bed pyrolysis reactor, which consists of a SUS 304 feedstock crucible that is loaded with 10 g of SP for each experiment and placed inside the reaction chamber. The reaction chamber is also made of SUS 304, which has a diameter of 10 cm and is 15 cm in height. N_2 carrier gas was streamed into the reactor system for 10 minutes before applying heat until pyrolysis was completed with a flow rate of 0.8 l/min. The reactor was heated using a gas stove until it reached 550℃ with a constant heating rate. The produced pyrolysis vapor produced was transferred into the water bath using a 100 cm 3/8"copper pipe and cooled down with a non-baffle condenser. The water bath functions as a secondary cooling unit and filters water-soluble compounds due to sensor working temperature requirements (<50°C). Water-soluble and other complex components need to be separated from non-condensable fractions to prevent sensor inlet blockage. The water bath was maintained at room temperature. Non-condensable vapor flows into a series of pre-calibrated MQ sensors to measure the concentration of hydrogen (MQ-8), methane (MQ-4), and carbon dioxide (MQ-135). Analog data from the sensor is then converted into digital data utilizing an Arduino Uno microcontroller and stored in a personal computer.

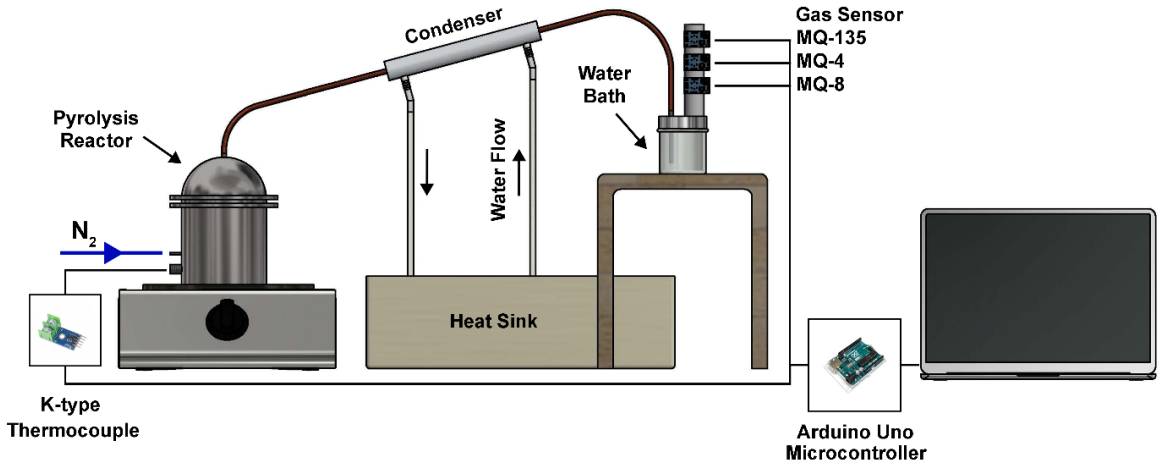

Fig. 1. Fixed-bed pyrolysis reactor

3. Thermogravimetry Analysis (TGA)

A non-isothermal TG/DTG analysis was carried out using the Mettler Toledo DSC 1 TGA apparatus to perform the pyrolysis of SP samples utilizing nitrogen as purging gas with a 100 ml/min flow rate. Pyrolysis temperature ranges of 25—900℃ were selected with 10, 20, 30, and 40℃/min heating rate variations.

4. Non-isothermal Kinetics Methods

Generally, the thermal degradation of SP microalgae generates volatile and char as the main product. Biomass pyrolysis is considered as a heterogeneous gas-solid reaction [26]. Its rate of reaction can be expressed using Eq. (1).

$$Biomass \xrightarrow{k(t)} Volatile\ (gas\ and\ tar) + Char\ (Solid\ Residue)$$

$$\frac{d\alpha}{dt} = k(T)f(\alpha) \quad \text{.....(1)}$$

where T is the reaction temperature, K; $k(T)$ is the reaction rate constant originating from the Arrhenius equation, as defined in Eq. (2); $f(\alpha)$ is the differential reaction function dependent on the reaction mechanism; α is conversion degree, described in Eq. (3).

$$k(T) = A\exp(-\frac{E_a}{RT}) \quad (2)$$

Arrhenius equation is useful for describing the rate constant of solid-state temperature-dependent reaction, encompassing phenomena such as diffusion, nucleation, and the growth of nuclei. Those behaviors happen presumably because the system has to overcome an energy barrier, and energy distribution along the relevant coordinates is controlled by Boltzmann statistics [26]. Therefore, A is frequency factor (s^{-1}); $\exp(-E_a/RT)$ is Boltzmann factor; E_a is apparent activation energy; R is universal gas constant ($8.314\ J/mol \cdot K$).

$$\alpha = \frac{m_i - m_T}{m_i - m_\infty} \quad (3)$$

α value obtained from the mass difference during the reaction. Where m_i is sample mass at initial reaction temperature; m_T is sample mass at a certain temperature; m_∞ is the final sample mass. A frequency factor is defined as:

$$A = \beta \times E_\alpha \frac{\exp(\frac{E_\alpha}{R \times Tm})}{R \times Tm^2} \quad (4)$$

where Tm is the peak decomposition temperature (K); K_B is Boltzmann constant; h is Planck constant ($6.626 \times 10^{-34} Js$).

Substituting reaction rate constant with Arrhenius formula into Eq. (5):

$$\frac{d\alpha}{dt} = A\exp(-\frac{E_a}{RT})f(\alpha) \quad (5)$$

$$\beta = \frac{dT}{dt} = \frac{dT}{d\alpha} \times \frac{d\alpha}{dt} \quad (6)$$

A constant term β, as described in Eq. (6) refers to the heating rate introduced as a conversion factor, used when required to alter the dynamic form into a non-isothermal form [26]. Converting Eq. (5) into Eq. (7).

$$\frac{d\alpha}{dT} = (\frac{A}{\beta})\exp(-\frac{E_a}{RT})f(\alpha) \quad (7)$$

Integrating Eq. (7) on both sides:

$$\int_0^\alpha \frac{d\alpha}{f(\alpha)} = g(\alpha) = \int_0^T \frac{A}{\beta}\exp(-\frac{E_a}{RT})dT \quad (8)$$

or

$$g(\alpha) = \int_0^{T_\alpha} \left(\frac{A}{\beta}\right)\exp\left(-\frac{E_a}{RT}\right)dT - \int_0^{T_0} \left(\frac{A}{\beta}\right)\exp\left(-\frac{E_a}{RT}\right)dT \quad (9)$$

The second term of Eq. (9) is comparatively small [26]. The general form of the integral iso-conversional kinetic methods after neglecting the low-temperature end of the interval described in Eq. (10).

$$g(\alpha) \approx \int_0^{T_\alpha} \left(\frac{A}{\beta}\right)\exp\left(-\frac{E_a}{RT}\right)dT = \left(\frac{A}{\beta R}\right)\int_0^\infty E_a \frac{\exp(-x)}{x^2}dx \quad (10)$$

when $x = E_a/RT_\alpha$

The g(α) is the integral form of the reaction model. Then, for non-isothermal TGA thermogram at a constant heating rate, Eq. (9) converts as below:

$$g(\alpha) = \frac{AE_a}{\beta R}\int_x^\infty \frac{e^{-x}}{x^2}dx = \frac{AE_a}{\beta R}p(x) \quad \text{.....(11)}$$

$p(x)$ is termed as exponential/temperature integral. At Eq. (11), $p(x) = p(E_a, T_\alpha)$. For a specific value of x, $p(x)$ has no analytical/exact solution [26]. However, various numerical approximation was proposed [27]–[29], and based on these studies, different mathematical expressions were derived for E_a estimation.

a. Kissinger-Akahira-Sunose (KAS)

KAS is an iso-conversional method employed to calculate the kinetic energy of SP. Applying the numerical approximation described in Eq. (12) in Eq. (11).

$$p(x) = x^{-2}e^{-x} \quad \text{.....(12)}$$

$$\ln\left(\frac{\beta}{T^2}\right) = \ln\frac{AR}{E_a g(\alpha)} - \frac{E_a}{RT} \quad \text{.....(13)}$$

$$\ln\left(\frac{\beta}{T^2}\right) = -\frac{E_a}{RT} \quad \text{.....(14)}$$

Eq. (14) is a general form of KAS model. Apparent E_a obtained from the slope of $\ln(\beta/T^2)$ versus $1/T$ plot, as described in Eq. (15), where m is the gradient multiplied by the universal gas constant.

$$E_a = m \times R \quad \text{.....(15)}$$

b. Ozawa-Flynn-Wall (OFW)

OFW is known as the model-free method [1]. Doyle's approximation, as expressed in Eq. (16), is used to calculate the activation energy and frequency factor of the material.

$$p(x) = -2.315 + 0.457x \quad \text{.....(16)}$$

Eq. (18) is a general form of OFW. E_a at a different conversion is acquired from the slope of $\ln\beta$ versus $1/T$, later substituting its gradient value into Eq. (19).

$$\ln(\beta) = \ln\frac{E_a A}{Rg(\alpha)} - 5{,}331 - 1{,}052\frac{E_a}{RT} \quad \text{.....(17)}$$

$$\ln(\beta) = 1{,}052\frac{E_a}{RT} \quad \text{.....(18)}$$

$$E_a = (m \times R)/1.0516 \quad \text{.....(19)}$$

c. Starink

Starink is considered a non-isothermal model-free method [1]. Gai et al. [30] reveal that the Starink method has higher accuracy compared to KAS and OFW. 'Ozawa's technique exhibits lower precision compared to KAS due to one order of magnitude. However, the KAS method achieves an error margin of 0.05%, while the Starink method output is five times more precise [29]. Eq. (20) originated from derived approximation.

$$\ln\left(\frac{\beta}{T^S}\right) = C_s - \frac{BE_a}{RT} \quad \text{.....(20)}$$

Substituting $S = 1.8$ and $B = 1.003$ in Eq. (20) can be written as below:

$$\ln\left(\frac{\beta}{T^{1.8}}\right) = C_s - 1{,}0037\frac{E_a}{RT} \quad \text{.....(21)}$$

$$\ln\left(\frac{\beta}{T^{1.8}}\right) = -1{,}0037\frac{E_a}{RT} \quad \text{.....(22)}$$

Eq. (22) is known as the Starink method. Linear graph plotting between $\ln(\beta/T^{1.8})$ versus $1/T$ produces a gradient that can be used with Eq. (23) to calculate the apparent E_a.

$$E_a = (m \times R)/1{,}0037 \quad \text{.....(23)}$$

5. Thermodynamics

Thermal phenomena during the pyrolysis process can be explained with thermodynamics parameter analysis. The change in enthalpy (ΔH) indicates a reaction process (endothermic or exothermic), the change in entropy (ΔS) indicates reaction system reactivity and the change in Gibbs free energy (ΔG) shows how far the system is from thermodynamic equilibrium [1]. Those thermodynamic parameters were calculated using the following equation:

$$\Delta H = E_\alpha - RT \quad \text{.....(24)}$$

$$\Delta G = E_\alpha + R \times Tm \times \ln\left(\frac{K_B \times Tm}{h \times A}\right) \quad \text{.....(25)}$$

$$\Delta S = \frac{\Delta H - \Delta G}{Tm} \quad \text{.....(26)}$$

III. Results and Discussions

1. Thermal Analysis

The result of the thermal degradation of SP at different heating rates has been presented in Figure 2a for the thermogravimetric (TG) graph. There are three general decomposition stages observed: moisture release or desorption of water (25—162.75℃), devolatilization (162.75—609.47℃), and carbonization (609.47—900℃). SP contains 8.25% moisture content, as shown with mass reduction at 162.75℃ [31]. The weight loss during the first stage is due to the removal of water or inbound moisture, and very low-temperature hydrocarbon is well documented [23]. The devolatilization process is the main decomposition zone of SP, indicated by 66.97% mass loss, the highest percentage compared to its counterpart. SP's main components are carbohydrates, proteins, and lipids with decomposition temperatures of 176—441, 211—564, and 216—302℃, respectively [32]. Those components degraded during the devolatilization stage, producing non-condensable gas through cracking, deoxygenation, and decarboxylation reaction [33]. SP residual mass consists of fixed carbon and ash with an average portion lower than 25%. As observed in the TG graph, heating variation does not change the decomposition behavior of SP.

The derivative thermogravimetric (DTG) graph (Figure 2b) reveals differences in decomposition rate with heating rate variation. As the heating rate increased, the maximum decomposition temperature (T_m) tend to be shifted to higher temperatures. Mass loss rate has a positive correlation with an incline of heating rate, with a maximum value of -0.043 mg/s at 40℃/min. That phenomenon is a result of thermal lag during pyrolysis throughout the cross-section of biomass particles, where short residence time did not allow enough time for interparticle heating [1], [34].

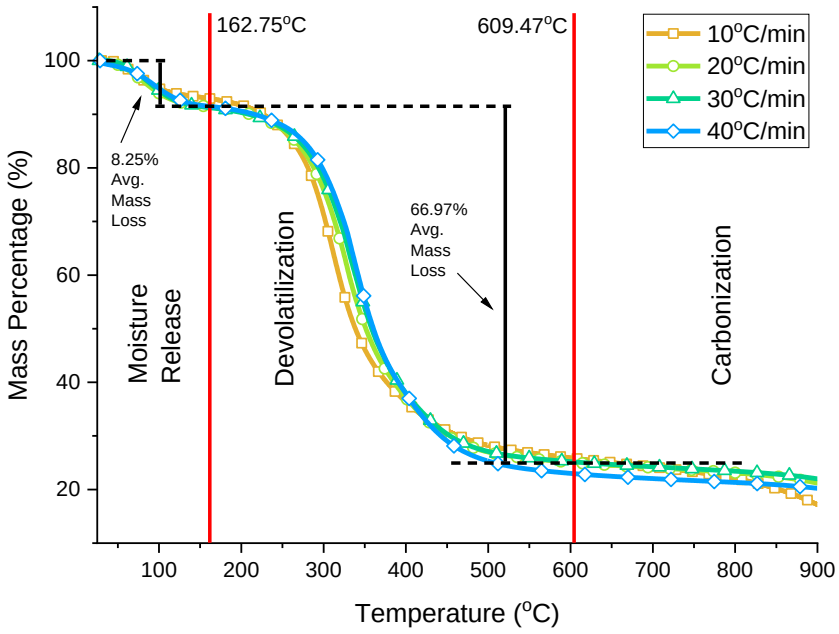

(a)

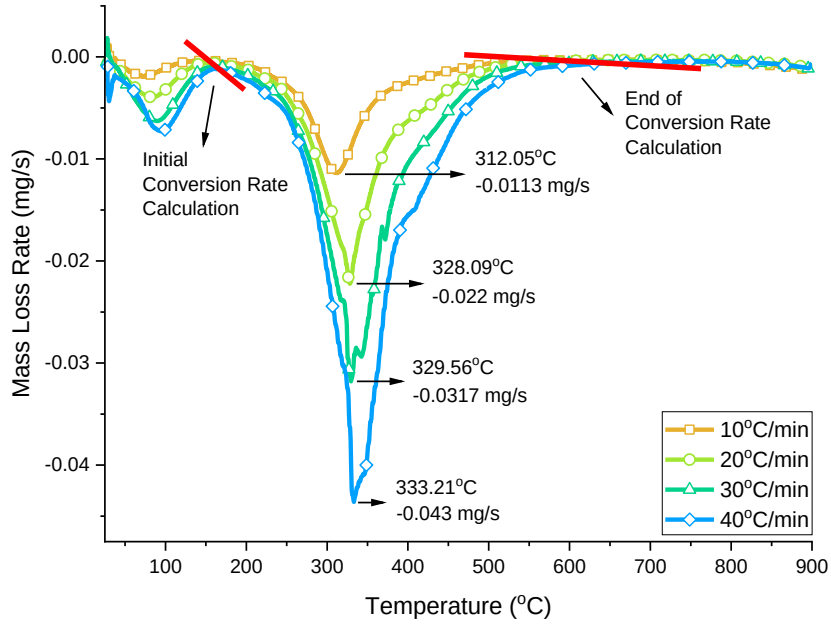

(b)

Fig. 2. Thermal behavior of SP during pyrolysis (a) TG and (b) DTG graph

2. Kinetics Analysis

Iso-conversional methods such as KAS, OFW, and Starink were used to determine the kinetic parameters such as activation energy and frequency factor. Iso-conversional kinetics parameter analysis requires conversion rate determination to calculate mass changes with respect to temperature [35]. The devolatilization zone was selected due to the significant decomposition that occurs in this process (Figure 2b), representing the SP component's conversion into volatile matter.

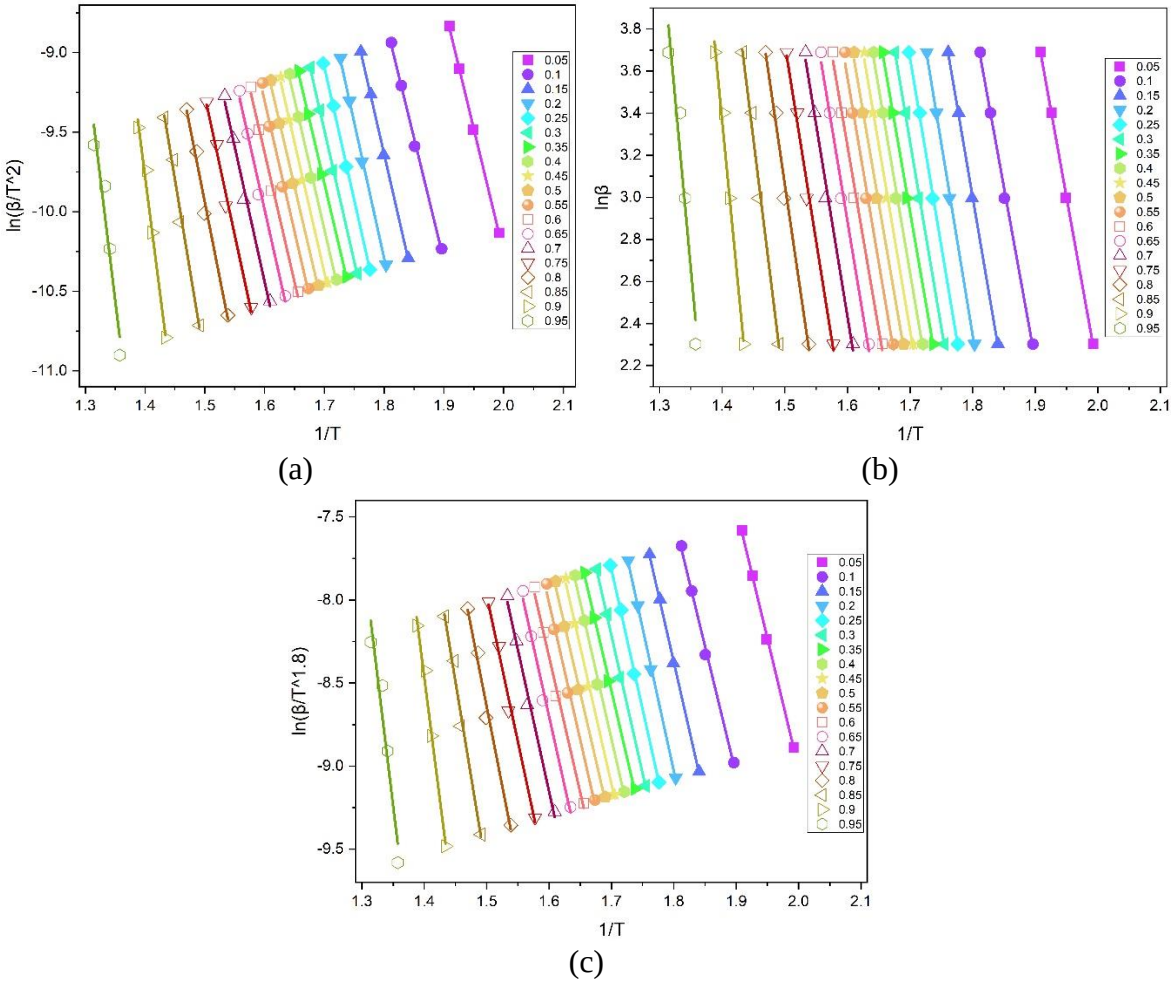

Fig. 3. Activation energy regression line plot of (a) KAS, (b) OFW, and (c) Starink

Figures 3a, b, and c depict the regression line plots of KAS, OFW, and Starink, respectively. OFW method has the best linear fit, resulting in the highest coefficient correlation (R^2) at 0.9918 compared to Starink and KAS. The average activation energy calculated from KAS, OFW, and Starink slope was 152.33, 154.56, and 152.78 kJ/mol, respectively (Table. 1). SP activation energy is comparatively lower than terrestrial biomass such as *Samanea saman* (188.28 kJ/mol), corn stalks (260.08 kJ/mol), pine sawdust (217.39 kJ/mol), and reed (231.5 kJ/mol) [1], [36]. Those results confirm that SP is suitable for pyrolysis feedstock and generates a good quantity of volatiles. An increase in Ea shows complex component degradation which is indicated by a relatively small change of mass at a certain temperature range as the devolatilization process is finished, leaving fixed carbon as a by-product due to volatile depletion [24], [37]. Fixed carbon decomposition requires more energy that promotes the activation energy increase when conversion nearly reaches 1 [25], [38]. Frequency factor (A) represents the probability of particle collision linked with reactivity at a given temperature. This frequency factor is directly related to the reaction as the reaction proceeds with the collision of particles [21]. The higher the frequency factor, the more complicated the reaction involved in the pyrolysis process [39], which was consistent with SP pyrolysis, where at the end of the devolatilization zone, the frequency factor value is rapidly increased due to exhaustion on volatile component and decomposing remaining complex component [25].

Table 1. Kinetics Analysis of SP

α	KAS			OFW			Starink		
	Ea (kJ/mol)	R^2	A (s^{-1})	Ea (kJ/mol)	R^2	A (s^{-1})	Ea (kJ/mol)	R^2	A (s^{-1})
0.05	129.44	0.999	1.93E+11	131.19	0.999	2.78E+11	129.81	0.999	2.08E+11
0.1	127.79	0.997	1.37E+11	130.03	0.997	2.18E+11	128.20	0.997	1.49E+11
0.15	136.29	0.999	8.03E+11	138.37	0.999	1.24E+12	136.70	0.999	8.76E+11
0.2	141.93	0.999	2.59E+12	143.92	0.999	3.93E+12	142.34	0.999	2.83E+12
0.25	139.03	0.999	1.42E+12	141.30	0.999	2.27E+12	139.47	0.999	1.55E+12
0.3	137.26	0.998	9.84E+11	139.73	0.999	1.64E+12	137.71	0.998	1.08E+12
0.35	133.04	0.998	4.09E+11	135.82	0.998	7.29E+11	133.52	0.998	4.52E+11
0.4	135.82	0.996	7.29E+11	138.55	0.996	1.28E+12	136.31	0.996	8.07E+11
0.45	136.39	0.995	8.20E+11	139.17	0.996	1.46E+12	136.88	0.995	9.08E+11
0.5	133.73	0.996	4.71E+11	136.74	0.997	8.82E+11	134.24	0.996	5.25E+11
0.55	136.16	0.992	7.83E+11	139.14	0.993	1.45E+12	136.67	0.992	8.70E+11
0.6	135.02	0.993	6.18E+11	138.18	0.994	1.19E+12	135.55	0.993	6.89E+11
0.65	139.15	0.989	1.45E+12	142.21	0.991	2.75E+12	139.67	0.989	1.62E+12
0.7	141.00	0.990	2.14E+12	144.14	0.992	4.10E+12	141.53	0.991	2.39E+12
0.75	145.02	0.989	4.93E+12	148.15	0.990	9.45E+12	145.55	0.989	5.50E+12
0.8	158.14	0.986	7.50E+13	160.88	0.988	1.32E+14	158.65	0.987	8.33E+13
0.85	188.88	0.986	4.31E+16	190.42	0.988	5.92E+16	189.32	0.986	4.72E+16
0.9	243.67	0.988	3.42E+21	242.92	0.989	2.93E+21	243.95	0.988	3.63E+21
0.95	256.46	0.929	4.75E+22	255.71	0.935	4.07E+22	256.75	0.930	5.04E+22
Avg.	152.33	0.990	2.68E+21	154.56	0.991	2.29E+21	152.78	0.991	2.84E+21

Table 2 enlist the comparison of SP average activation energy with other reported literature using iso-conversional methods. Simão et al. [40] calculated SP pyrolysis kinetics using OFW methods, where the obtained activation energy is 143.77 kJ/mol, lower than present study findings with an interval of 10.76 kJ/mol. However, Ea differences between methods are common in kinetics calculation, as suggested by Soen et al. [20].

Table 2. SP Apparent Activation Energy Comparison

Methods	Activation Energy (kJ/mol)	Reference
OFW	154.56	This work
Differential	109—340	[41]
Integral	102—272	
OFW	143.77	[40]
Friedman	132.62	
Miura-Maki	136.89	
Freeman-Caroll	76—97	[42]
Vyazovkin	74.4—140.1	[43]

3. Thermodynamics Analysis

Table 3 shows thermodynamic parameters such as enthalpy, entropy, and Gibbs free energy, calculated using apparent activation energy from OFW methods due to its suitability for SP pyrolysis. The amount of energy exchanged during a chemical reaction is known as enthalpy. Pyrolysis feedstock conversion into gas, liquid, and solid products requires sufficient enthalpy, which implies the energy difference between the activated complex (transition state) and the reagent [44]. Activation energy and enthalpy comparison show a

small potential energy barrier (5.13 kJ/mol), indicating the reaction viability at that condition. Xu et al. [44] reveal that small intervals between activation energy and enthalpy imply that the formation of an activation complex is favorable, whereby providing a small amount of additional energy, the product formation will be achieved. However, a positive value of ΔH indicates a non-spontaneous reaction.

Entropy implies a degree of disorder that represents the reactivity of a system. The average entropy value is -0.09J/mol.K, and negative entropy was also reported in the previous study [38], [45], [46]. A negative sign shows low reactivity and vice versa. Thereby, the reaction is unfavorable and requires energy input to sustain the reaction [47].

Gibbs energy represents the amount of energy available from the material [1]; its changes imply that the 'system's overall energy rises as the reagents approach to convert into the activated form [48]. Gibbs energy shows a positive value, indicating a non-spontaneous reaction where external energy is needed to sustain the reaction [49].

Table 3. Thermodynamics Parameter of OFW Methods

Temperature (℃)	(α)	ΔH (kJ/mol)	ΔG^0 (kJ/mol)	ΔS (J/mol.K)
241.4	0.05	126.91	150.20	-38.90
268.5	0.1	125.53	150.24	-41.28
284.3	0.15	133.74	149.93	-27.05
295.7	0.2	139.20	149.74	-17.61
304.6	0.25	136.50	149.83	-22.27
312.1	0.3	134.87	149.88	-25.08
318.7	0.35	130.90	150.03	-31.95
324.5	0.4	133.58	149.93	-27.30
330.0	0.45	134.16	149.90	-26.30
335.8	0.5	131.68	149.99	-30.60
341.8	0.55	134.03	149.91	-26.52
348.8	0.6	133.01	149.94	-28.29
356.7	0.65	136.97	149.80	-21.42
366.6	0.7	138.82	149.73	-18.22
379.1	0.75	142.73	149.59	-11.46
394.5	0.8	155.33	149.18	10.27
413.2	0.85	184.71	148.34	60.75
436.9	0.9	237.01	147.13	150.14
475.2	0.95	249.49	146.88	171.40
Avg.		149.43	149.48	-0.09

4. Non-condensable Gas Yield and Its Correlation with Activation Energy

Gas formation characteristics from SP pyrolysis using a fixed-bed reactor are analyzed with an MQ series sensor. Table 4. shows the average non-condensable gas concentration during pyrolysis. Gas product distribution is dominated by CH_4, indicating SP has the potential to be used as a gaseous fuel feedstock. Those results are in line with Chernova et al. [11] findings where Spirulina non-condensable product dominated by C_xH_y fraction.

The non-condensable gas concentration is dependent on biomass component degradation temperature, as shown in Figure 4. At 310℃, all non-condensable gas production surges due to the maximum decomposition rate have been achieved (Figure 2b). Based on a literature study, carbohydrate and protein decomposition mainly produced H_2 [33]. CH_4 is also generated from those degraded components. However, lipid is also one of

the CH_4 product contributors; as visualized in Figure 3b, the production of CH_4 shows an inclining trend during lipid decomposition temperature. The generation of CH_4 is due to a methanation reaction that occurs, as indicated by many researchers. CO_2 is generated through carbohydrate decomposition due to its vast amount of oxygen compound [50]. This theory confirmed the CO_2 production decline at the end of the carbohydrate decomposition zone (441℃). The CO_2 formation is caused by a decarboxylation reaction. Xu et al. [44] found that protein decomposed at a higher conversion degree than cellulose.

Table 4. Non-condensable gas production of SP pyrolysis

Gas Product Species	Average Concentration (ppm)
Hydrogen (H_2)	3775.212
Methane (CH_4)	83792.19
Carbon Dioxide (CO_2)	23592.58

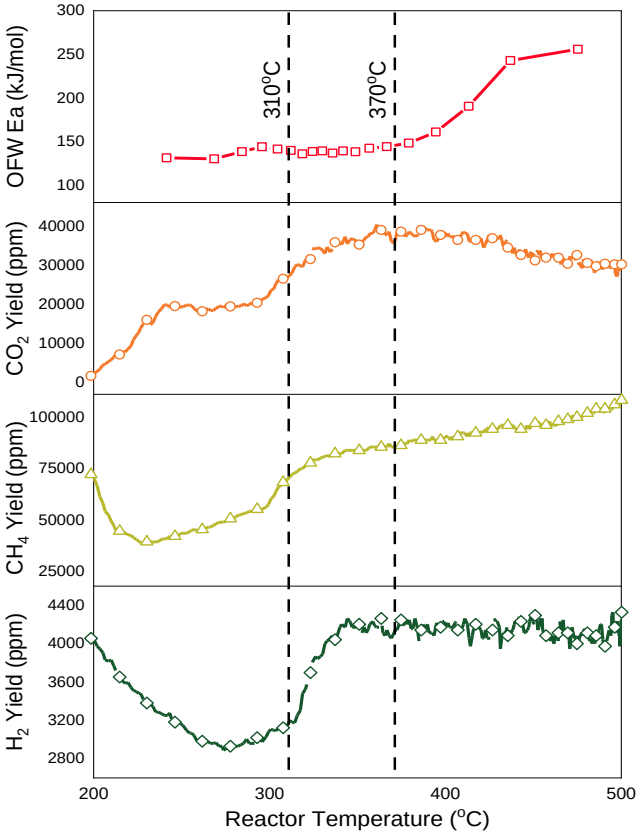

Fig. 4. Apparent activation energy correlation with SP non-condensable gas production

The calculated activation energy forms a plateau trend on conversion (α) of 0.05—0.75 and begins to increase until $\alpha = 0.95$. Those phenomena can be explained by the decomposition temperature of the SP main component, where easy to decompose components tend to have lower activation energy than their counterparts due to their rapid mass changes in narrow temperature ranges [24]. The temperature range of 0.05—0.75 conversion is 241.47—379.16℃, exactly the same as the decomposition temperature of the three SP's main components. This indicates the easy convertibility of SP from solid to gas phase during pyrolysis. However, 0.8—0.95 conversion has a temperature range of

394.56—475.28℃ where lipid and carbohydrate are already or almost completely decomposed, and only protein exists until the temperature of 564℃. Activation energy increase is due to a higher amount of energy required for the decomposition of material such as protein and other complex materials [25].

The activation energy needed for decomposing for carbohydrates, lipids, and proteins ranges from 50.07—207.3, 45.59—146.06, and 126.69—304.61 kJ/mol, respectively [51]. As listed in Table 1, lipids already decomposed at $\alpha = 0.15$, carbohydrates at $\alpha = 0.85$, and protein lasted until the end of the conversion degree. Those findings are inline with the decomposition temperature of SP components, where protein is the main contributor for CH_4 generation, which is indicated by production incline during $\alpha = 0.9$—0.95. H_2 production was dependent on carbohydrate decomposition, increasing until reaching stagnation at $\alpha = 0.6$ due to mass loss rate decline (Figure 4) and carbohydrate depletion. However, protein also contributes to H_2 generation, though it does not increase its production rate. Carbon dioxide yield decreased at $\alpha = 0.75$, near the end of the carbohydrate activation energy barrier (207.3 kJ/mol), confirming that CO_2 yield is dependent on the degradation of carbohydrates. As shown in Figure 4, the optimum SP pyrolysis temperature ranges between 310—370℃ or in terms of conversion rate is $\alpha = 0.3$—0.7, where activation energy is relatively low (139.29 kJ/mol) accompanied by a rapid increase of H_2 and CH_4 yield.

IV. Conclusions

The optimal SP pyrolysis temperature is required to develop better economic, energy, and desired product yield efficiency. The activation energies of KAS, OFW, and Starink are 152.33, 154.56, and 152.78 kJ/mol, respectively. Thermodynamic analysis was conducted using the OFW method due to its highest R^2 of 0.9918. The average enthalpy is 149.43 kJ/mol with an energy barrier of 5.13 kJ/mol. The Entropy of SP pyrolysis is -0.09 J/mol.K on average. Gibbs energy mean value is 149.48 kJ/mol, and those thermodynamic parameters indicate that SP pyrolysis is unfavorable and requires energy input to sustain the reaction. Non-condensable gasses produced during pyrolysis are composed of H_2 (3775.21 ppm), CH_4 (83792.19 ppm), and CO_2 (23592.58 ppm). Combining kinetics analysis with non-condensable gas yield, the optimum SP decomposition temperature is 310—370℃ or in terms of conversion rate is $\alpha = 0.3$—0.7, where average activation energy is 139.29 kJ/mol along with rapid non-condensable gas generation. However, those temperatures only apply in non-condensable gas production. This study can provide -additional information for optimizing SP pyrolysis reactor parameters.

Acknowledgment

This research was financially supported by a DRPTM research grant for the Magister Thesis with a contract number of 140/E5/PG.02.00.PL/2023.

References

[1] R.K. Mishra, A. Sahoo, and K. Mohanty, “Pyrolysis kinetics and synergistic effect in co-pyrolysis of Samanea saman seeds and polyethylene terephthalate using thermogravimetric analyser,” *Bioresour. Technol.*, vol. 289, no. April, p. 121608, 2019, doi: 10.1016/j.biortech.2019.121608.

[2] K.G. Burra and A.K. Gupta, “Kinetics of synergistic effects in co-pyrolysis of biomass with plastic wastes,” *Appl. Energy*, vol. 220, no. October 2017, pp. 408–418, 2018, doi: 10.1016/j.apenergy.2018.03.117.

[3] M. Shahbaz, A. Al-Nouss, I. Ghiat, G. Mckay, H. Mackey, S. Elkhalifa, and T. Al-Ansari, "A comprehensive review of biomass based thermochemical conversion technologies integrated with CO_2 capture and utilisation within BECCS networks," *Resour. Conserv. Recycl.*, vol. 173, p. 105734, 2021, doi: https://doi.org/10.1016/j.resconrec.2021.105734.

[4] M. Shahbaz, N. Rashid, J. Saleem, H. Mackey, G. McKay, and T. Al-Ansari, "A review of waste management approaches to maximise sustainable value of waste from the oil and gas industry and potential for the state of Qatar," *Fuel*, vol. 332, p. 126220, 2023, doi: https://doi.org/10.1016/j.fuel.2022.126220.

[5] A.T. Hoang, H.C. Ong, I.M.R. Fattah, C.T. Chong, C.K. Cheng, R. Sakthivel, and Y.S. Ok, "Progress on the lignocellulosic biomass pyrolysis for biofuel production toward environmental sustainability," *Fuel Process. Technol.*, vol. 223, p. 106997, 2021, doi: https://doi.org/10.1016/j.fuproc.2021.106997.

[6] E.T. Kostas, J.M. M. Adams, H.A. Ruiz, G. Durán-Jiménez, and G.J. Lye, "Macroalgal biorefinery concepts for the circular bioeconomy: A review on biotechnological developments and future perspectives," *Renew. Sustain. Energy Rev.*, vol. 151, p. 111553, 2021, doi: https://doi.org/10.1016/j.rser.2021.111553.

[7] M. Shahbaz, A. Al-Nouss, P. Parthasarathy, A.H. Abdelaal, H. Mackey, G. McKay, and T. Al-Ansari, "Investigation of biomass components on the slow pyrolysis products yield using Aspen Plus for techno-economic analysis," *Biomass Convers. Biorefinery*, vol. 12, no. 3, pp. 669–681, 2022, doi: 10.1007/s13399-020-01040-1.

[8] Y.H. Chan, K.W. Cheah, B.S. How, A.C.M. Loy, M. Shahbaz, H.K.G. Singh et al., "An overview of biomass thermochemical conversion technologies in Malaysia," *Sci. Total Environ.*, vol. 680, pp. 105–123, 2019, doi: https://doi.org/10.1016/j.scitotenv.2019.04.211.

[9] V. Anand, V. Sunjeev, and R. Vinu, "Catalytic fast pyrolysis of *Arthrospira platensis* (spirulina) algae using zeolites," *J. Anal. Appl. Pyrolysis*, vol. 118, pp. 298–307, 2016, doi: 10.1016/j.jaap.2016.02.013.

[10] H. Desmorieux, J. Madiouli, C. Herraud, and H. Mouaziz, "Effects of size and form of *Arthrospira Spirulina* biomass on the shrinkage and porosity during drying," *J. Food Eng.*, vol. 100, no. 4, pp. 585–595, 2010, doi: https://doi.org/10.1016/j.jfoodeng.2010.03.021.

[11] N.I. Chernova, S.V. Kiseleva, O.M. Larina, and G.A. Sytchev, "Manufacturing gaseous products by pyrolysis of microalgal biomass," *Int. J. Hydrogen Energy*, vol. 45, no. 3, pp. 1569–1577, 2020, doi: 10.1016/j.ijhydene.2019.11.022.

[12] N.I. Chernova, S.V. Kiseleva, and O.S. Popel', "Efficiency of the biodiesel production from microalgae," *Therm. Eng.*, vol. 61, no. 6, pp. 399–405, 2014, doi: 10.1134/S0040601514060019.

[13] D. Soletto, L. Binaghi, A. Lodi, J.C.M. Carvalho, and A. Converti, "Batch and fed-batch cultivations of *Spirulina platensis* using ammonium sulphate and urea as nitrogen sources," *Aquaculture*, vol. 243, no. 1, pp. 217–224, 2005, doi: https://doi.org/10.1016/j.aquaculture.2004.10.005.

[14] S. Sukarni and M.R. Ramadhan, "Pyrolytic characteristics and kinetic parameters evaluation of cassava stalks using thermogravimetric analyzer," *Key Eng. Mater.*, vol. 851 KEM, pp. 137–141, 2020, doi: 10.4028/www.scientific.net/KEM.851.137.

[15] M.A. Adnan and M.M. Hossain, "Integrated drying and gasification of wet microalgae biomass to produce H_2 rich syngas – A thermodynamic approach by considering in-situ energy supply," *Int. J. Hydrogen Energy*, vol. 44, no. 21, pp. 10361–10373, 2019, doi: 10.1016/j.ijhydene.2019.02.165.

[16] Y. Zakaria, S. Sukarni, P. Puspitasari, and N. Mufti, "Investigate the potential renewable energy of microalgae Spirulina sp," vol. 6, no. 2, pp. 66–73, 2022, doi: 10.17977/um016v6i22022p066.
[17] D.O. Patrick, S. Yusup, N.B. Osman, H. Zabiri, Y. Uemura, and M. Shahbaz, "Thermogravimetric kinetics of catalytic and non-catalytic pyrolytic conversion of palm kernel shell with acid-treated coal bottom ash," *BioEnergy Res.*, vol. 13, no. 2, pp. 452–462, 2020, doi: 10.1007/s12155-020-10101-2.
[18] R. Sharma, P.N. Sheth, and A.M. Gujrathi, "Kinetic modeling and simulation: Pyrolysis of Jatropha residue de-oiled cake," *Renew. Energy*, vol. 86, pp. 554–562, 2016, doi: 10.1016/j.renene.2015.08.066.
[19] M. Hu, X. Wang, J. Chen, P. Yang, C. Liu, B. Xiao, and D. Guo, "Kinetic study and syngas production from pyrolysis of forestry waste," *Energy Convers. Manag.*, vol. 135, pp. 453–462, 2017, doi: 10.1016/j.enconman.2016.12.086.
[20] S. Steven, P. Hernowo, N. Nadirah, I. Febijanto, R. Herdioso, D. Dharmawan et al., "Transformation method in determining kinetic parameters of biomass thermal decomposition from solid-state approach to volatile state approach," *Biomass and Bioenergy*, vol. 183, no. February, p. 107171, 2024, doi: 10.1016/j.biombioe.2024.107171.
[21] S. Sukarni, "Thermogravimetric analysis of the combustion of marine microalgae *Spirulina platensis* and its blend with synthetic waste," *Heliyon*, vol. 6, no. 9, 2020, doi: 10.1016/j.heliyon.2020.e04902.
[22] T. Suprianto, Winarto, W. Wijayanti, and I.N.G. Wardana, "Synergistic effect of curcumin and activated carbon catalyst enhancing hydrogen production from biomass pyrolysis," *Int. J. Hydrogen Energy*, vol. 46, no. 10, pp. 7147–7164, 2021, doi: 10.1016/j.ijhydene.2020.11.211.
[23] R. Tariq, A. Inayat, M. Shahbaz, H. Zeb, C. Ghenai, T. Al-Ansari, and J. Kim, "Kinetic and thermodynamic evaluation of pyrolysis of jeans waste via coats-redfern method," *Korean J. Chem. Eng.*, vol. 40, no. 1, pp. 155–161, 2023, doi: 10.1007/s11814-022-1248-3.
[24] T.W. Yacob, R. (Chip) Fisher, K.G. Linden, and A.W. Weimer, "Pyrolysis of human feces: Gas yield analysis and kinetic modeling," *Waste Manag.*, vol. 79, pp. 214–222, 2018, doi: 10.1016/j.wasman.2018.07.020.
[25] L. Qin, J. Han, B. Zhao, W. Chen, and F. Xing, "The kinetics of typical medical waste pyrolysis based on gaseous evolution behaviour in a micro-fluidised bed reactor," *Waste Manag. Res.*, vol. 36, no. 11, pp. 1073–1082, 2018, doi: 10.1177/0734242X18790357.
[26] A. Sharma and B. Mohanty, "Thermal degradation of mango (*Mangifera indica*) wood sawdust in a nitrogen environment: characterization, kinetics, reaction mechanism, and thermodynamic analysis," *RSC Adv.*, vol. 11, no. 22, pp. 13396–13408, 2021, doi: 10.1039/d1ra01467f.
[27] H.E. Kissinger, "Variation of peak temperature with heating rate in differential thermal analysis," *J. Res. Natl. Bur. Stand. (1934).*, vol. 57, no. 4, p. 217, 1956, doi: 10.6028/jres.057.026.
[28] T. Ozawa, "Estimation of activation energy by isoconversion methods," *Thermochim. Acta*, vol. 203, no. C, pp. 159–165, 1992, doi: 10.1016/0040-6031(92)85192-X.
[29] M.J. Starink, "A new method for the derivation of activation energies from experiments performed at constant heating rate," *Thermochim. Acta*, vol. 288, no. 1–2, pp. 97–104, 1996, doi: 10.1016/s0040-6031(96)03053-5.
[30] C. Gai, Y. Dong, and T. Zhang, "The kinetic analysis of the pyrolysis of agricultural

residue under non-isothermal conditions," *Bioresour. Technol.*, vol. 127, pp. 298–305, 2013, doi: 10.1016/j.biortech.2012.09.089.

[31] Sukarni, Sudjito, N. Hamidi, U. Yanuhar, and I.N.G. Wardana, "Potential and properties of marine microalgae Nannochloropsis oculata as biomass fuel feedstock," *Int. J. Energy Environ. Eng.*, vol. 5, no. 4, pp. 279–290, 2014, doi: 10.1007/s40095-014-0138-9.

[32] W.H. Chen, Y.S. Chu, J.L. Liu, and J.S. Chang, "Thermal degradation of carbohydrates, proteins and lipids in microalgae analyzed by evolutionary computation," *Energy Convers. Manag.*, vol. 160, no. January, pp. 209–219, 2018, doi: 10.1016/j.enconman.2018.01.036.

[33] B.M.E. Chagas, C. Dorado, M.J. Serapiglia, C.A. Mullen, A.A. Boateng, M.A.F. Melo, and C.H. Ataíde, "Catalytic pyrolysis-GC/MS of Spirulina: Evaluation of a highly proteinaceous biomass source for production of fuels and chemicals," *Fuel*, vol. 179, pp. 124–134, 2016, doi: 10.1016/j.fuel.2016.03.076.

[34] P.O. Okekunle, H. Watanabe, T. Pattanotai, and K. Okazaki, "Effect of biomass size and aspect ratio on intra-particle tar decomposition during wood cylinder pyrolysis," *J. Therm. Sci. Technol.*, vol. 7, no. 1, pp. 1–15, 2012, doi: 10.1299/jtst.7.1.

[35] E. Tarani and K. Chrissafis, "Isoconversional methods: A powerful tool for kinetic analysis and the identification of experimental data quality," *Thermochim. Acta*, vol. 733, no. December 2023, p. 179690, 2024, doi: 10.1016/j.tca.2024.179690.

[36] J. Li, Y. Shang, W. Wei, Z. Liu, Y. Qiao, S. Qin, and Y. Tian, "Comparative study on pyrolysis kinetics behavior and high-temperature fast pyrolysis product analysis of coastal zone and land biomasses," *ACS Omega*, vol. 7, no. 12, pp. 10144–10155, 2022, doi: 10.1021/acsomega.1c06363.

[37] A. Al-Rumaihi, M. Shahbaz, G. Mckay, H. Mackey, and T. Al-Ansari, "A review of pyrolysis technologies and feedstock: A blending approach for plastic and biomass towards optimum biochar yield," *Renew. Sustain. Energy Rev.*, vol. 167, no. May, p. 112715, 2022, doi: 10.1016/j.rser.2022.112715.

[38] O. Fischer, R. Lemaire, and A. Bensakhria, "Thermogravimetric analysis and kinetic modeling of the pyrolysis of different biomass types by means of model-fitting, model-free and network modeling approaches," *J. Therm. Anal. Calorim.*, no. 0123456789, 2024, doi: 10.1007/s10973-023-12868-w.

[39] K. Wang, T. Shan, B. Li, Y. Zheng, H. Xu, C. Wang, and X. Tian, "Study on pyrolysis characteristics, kinetics and thermodynamics of waste tires catalytic pyrolysis with low-cost catalysts," *Fuel*, vol. 356, no. August 2023, p. 129644, 2024, doi: 10.1016/j.fuel.2023.129644.

[40] B.L. Simão, J.A.S. Júnior, B.M.E. Chagas, C.R. Cardoso, and C.H. Ataíde, "Pyrolysis of Spirulina maxima: Kinetic modeling and selectivity for aromatic hydrocarbons," *Algal Res.*, vol. 32, no. October 2017, pp. 221–232, 2018, doi: 10.1016/j.algal.2018.04.007.

[41] V. Vasudev, X. Ku, and J. Lin, "Pyrolysis of algal biomass: Determination of the kinetic triplet and thermodynamic analysis," *Bioresour. Technol.*, vol. 317, no. August, p. 124007, 2020, doi: 10.1016/j.biortech.2020.124007.

[42] Q.V. Bach and W.H. Chen, "Pyrolysis characteristics and kinetics of microalgae via thermogravimetric analysis (TGA): A state-of-the-art review," *Bioresour. Technol.*, vol. 246, pp. 88–100, 2017, doi: 10.1016/j.biortech.2017.06.087.

[43] C. Gai, Y. Zhang, W.T. Chen, P. Zhang, and Y. Dong, "Thermogravimetric and kinetic analysis of thermal decomposition characteristics of low-lipid microalgae," *Bioresour. Technol.*, vol. 150, pp. 139–148, 2013, doi:

10.1016/j.biortech.2013.09.137.

[44] Y. Xu and B. Chen, "Investigation of thermodynamic parameters in the pyrolysis conversion of biomass and manure to biochars using thermogravimetric analysis," *Bioresour. Technol.*, vol. 146, pp. 485–493, 2013, doi: 10.1016/j.biortech.2013.07.086.

[45] S.L. Narnaware and N.L. Panwar, "Kinetic study on pyrolysis of mustard stalk using thermogravimetric analysis," *Bioresour. Technol. Reports*, vol. 17, no. January, p. 100942, 2022, doi: 10.1016/j.biteb.2021.100942.

[46] S.A. El-Sayed, T.M. Khass, and M.E. Mostafa, "Thermal degradation behaviour and chemical kinetic characteristics of biomass pyrolysis using TG/DTG/DTA techniques," *Biomass Convers. Biorefinery*, no. 0123456789, pp. 20–40, 2023, doi: 10.1007/s13399-023-03926-2.

[47] R. Chang and J. Overby, *General Chemistry: The Essential Concepts*. McGraw-Hill, 2011.

[48] S.C. Turmanova, S.D. Genieva, A.S. Dimitrova, and L.T. Vlaev, "Non-isothermal degradation kinetics of filled with rise husk ash polypropene composites," *Express Polym. Lett.*, vol. 2, no. 2, pp. 133–146, 2008, doi: 10.3144/expresspolymlett.2008.18.

[49] J. Yan, Q. Yang, L. Zhang, Z, Lei, Z. Li, Z. Wang, et al., "Investigation of kinetic and thermodynamic parameters of coal pyrolysis with model-free fitting methods," *Carbon Resour. Convers.*, vol. 3, no. November, pp. 173–181, 2020, doi: 10.1016/j.crcon.2020.11.002.

[50] M.P.B. Martins, C.E. Hori, M.A.S. Barrozo, and L.G.M. Vieira, "Solar Pyrolysis of *Spirulina platensis* Assisted by Fresnel Lens Using Hydrocalumite-Type Precursors," *Energies*, vol. 15, no. 20, 2022, doi: 10.3390/en15207590.

[51] R. Aniza, W.-H Chen, Y.-Y. Lin, K.-Q. Tran, J.-S. Chang, S.S. Lam, et al., "Independent parallel pyrolysis kinetics of extracted proteins and lipids as well as model carbohydrates in microalgae," *Appl. Energy*, vol. 300, no. April, p. 117372, 2021, doi: 10.1016/j.apenergy.2021.117372.